SF2A 2007
J. Bouvier, A. Chalabaev, C. Charbonnel (eds)

THE PROMPT HIGH-ENERGY GAMMA-RAY EMISSION FROM GRBS: PREDICTIONS FOR GLAST

Z. Bosnjak[1], F. Daigne[1], G. Dubus[2], B. Giebels[3] and F. Piron[4]

Abstract. We compute the prompt high-energy gamma-ray emission from GRBs in the framework of the internal shock model. For this purpose we combine a code developed to follow the dynamics of the internal shock phase with a code dealing with high-energy radiative processes. We present our first results and discuss them in the prospect of future GLAST observations.

1 Introduction

The proximity of the *Gamma–ray Large Area Space Telescope* (GLAST) mission launch schedule has prompted the urge for the detailed study of the high energy (in the range of GeV and higher) gamma–ray burst (GRB) emission. Current observational informations on very high-energy gamma–rays emitted in a gamma–ray burst date from the *Energetic Gamma–Ray Experiment Telescope* (EGRET) mission on board the *Compton Gamma Ray Observatory* (CGRO). It covered the energy band 20 MeV - 30 GeV and detected the high energy photons from a handful of GRBs; the most energetic (18 GeV) photon was detected in case of GRB 940217 (Hurley et al. 1994). The inspection of the data sets for gamma–ray bursts (7 events, see e.g. Baring 2006) that were seen by two detectors on CGRO, EGRET and *Burst and Transient Source Experiment* (BATSE), indicates that these events were among the brightest ones detected by BATSE (the observed fluence $>1.2 \times 10^{-5}$erg cm^{-2} and the photon flux >6.2 photon cm^{-2} s^{-1} in 50-300 keV range) (see e.g. Paciesas et al. 1999). The evidence for even higher (TeV) energy emission from GRBs was reported from the ground-based experiments, based on the detection of the extensive air showers produced by the high energy photons in the atmosphere (e.g. Atkins et al. 2000).

GRBs are believed to be produced by ultra-relativistic ($\Gamma \gtrsim 100$) outflows ejected from a new formed compact stellar mass source. The prompt gamma-ray emission is usually interpreted as radiation from accelerated electrons in shock waves that propagate within the outflow (Rees & Mészáros 1994). Such "internal" shocks can form if the ejection process by the central source is highly variable. The high energy spectral component is expected naturally within this framework. The typical GRB spectrum in the low gamma-ray range, as observed for instance by BATSE, is a smoothly connected broken power law with a break energy in the range 0.1 - 1 MeV. This component is probably directly produced by synchrotron radiation from the shock accelerated electrons. Thus observations of the GRB spectrum extending to very high energy emission (GeV ranges) can be expected when the synchrotron photons are inverse Compton scattered (provided that the $\gamma\gamma$ opacity in the source is small). Depending on the relevant parameters, the flux of the high energy component can be even comparable to the prompt GRB gamma–ray flux in BATSE energy range.

In view of the significant observational advances expected with the launch of GLAST, we have performed the detailed calculation of gamma–ray burst prompt emission in the context of the internal shocks scenario, focusing on the high energy (GeV) band.

[1] Institut d'Astrophysique de Paris, UMR 7095 CNRS - Université Pierre et Marie Curie-Paris 6, 98 bis boulevard Arago, 75014 Paris, France

[2] Laboratoire d'Astrophysique de Grenoble, Université J. Fourier, CNRS, BP 53, 38041 Grenoble, France

[3] Laboratoire Leprince-Ringuet, UMR 7638 CNRS, École Polytechnique, 91128 Palaiseau, France

[4] Laboratoire de physique théorique et astroparticules (UMR 5207 CNRS/IN2P3), Université Montpellier 2, 34095 Montpellier, France

2 Model: high energy emission in the internal shocks scenario

In order to follow the time evolution of the gamma–ray spectrum emerging from the relativistic outflow during the internal shock phase, several steps are needed:

1. The dynamics of the internal shock phase must be followed to determine the physical conditions behind each shock wave;

2. In the shocked medium, electrons are accelerated and the magnetic field is amplified. The emitted photon spectrum has to be computed from the time-dependant evolution of the relativistic electrons. This evolution is governed by several radiative processes that are in competition with the adiabatic cooling due to the spherical expansion.

3. From the evolution of the emission in the comoving frame of the shocked material, one can deduce the observed light-curve and spectrum and produce a "synthetic" GRB.

A simplified version of this difficult project has already been presented by several authors, who focus on the second step (radiative processes in the comoving frame) after assuming a typical collision between two relativistic shells for the first step. For instance, Asano & Inoue 2007, also Gupta & Zhang 2007, have recently discussed the different emission mechanisms of high energy photon production during internal shocks and derived the expected high energy photon spectrum from one single shocked relativistic shell. In this work we attempt to improve this approach by combining a complete model for the dynamics of the internal shocks with a detailed calculation of the relevant radiative processes occurring in the shocked medium. This allows us for the first time to obtain the time evolution of the high-energy gamma-ray emission in a GRB.

2.1 Dynamics of internal shocks

The evolution of the ultra relativistic outflow is followed using the model developed by Daigne & Mochkovitch 1998. They consider a discretized wind consisting of a succession of shells ejected every Δt seconds with a varying Lorentz factor Γ, during a total time of the energy injection t_w. They also assume a constant kinetic energy injection rate. As the wind expands, the shells progressively collide with each other and merge in the collisions. Fig 1. shows an example of such a dynamical simulation for a simple case where the ejected outflow is made of a slow and a rapid part. This simple distribution results in a single pulse GRB. The successive collisions simulate the two shock waves propagating in the outflow. The evolution is followed until all the shells are ordered with Γ decreasing from the front to the rear part. The efficiency of the internal shock process is rather low: 10-40 % of the kinetic energy of the outflow can be converted in internal energy, but only a fraction of this can be radiated in gamma-rays.

The input parameters of our model are the distribution of Lorentz factors Γ(t) and the kinetic energy rate $\dot{E}(t)$ during the relativistic ejection, and the total duration t_w of this phase (this timescale reflects the duration of the activity of the central engine). The code follows the dynamics of all the discretized shells. A typical distance at which the shocks take place in this model ranges from $\sim 10^{11}$ to $\sim 10^{15}$ cm. The shocks are only mildly relativistic so that the typical energy dissipated in a collision of two shells is of the order of 200 MeV per proton. We do not consider in this work the details of the acceleration mechanism by shock waves. We assume that this dissipated energy is distributed in a fraction α_e which is injected in relativistic electrons (with a number density that follows a power-law : $n'(\Gamma_e) \sim \Gamma_e^{-p}$ for $\Gamma_e \geq \Gamma_m$) and a fraction α_B which is injected in the random magnetic field amplified by the shock wave ($\alpha_e + \alpha_B < 1$). In addition, we assume that the energy injected in electrons is selectively injected in only a (number) fraction ξ of all electrons (see Bykov & Mészáros 1996). Therefore, most of the electrons are not accelerated, but however still contribute to the Thomson optical depth of the shell.

For each collision the physical conditions in the shocked medium are computed (Fig 2.): the Lorentz factor Γ_*, the comoving density ρ_* and the comoving specific energy density ϵ_* of the shocked medium. The plots of these quantities have two branches, corresponding to collisions associated to the two propagating shocks (see Fig.1). The inferred magnetic field B is also shown, as well as the typical Lorentz factor of the electrons, Γ_m. In the following we consider the cooling of the electron distribution and the associated emission.

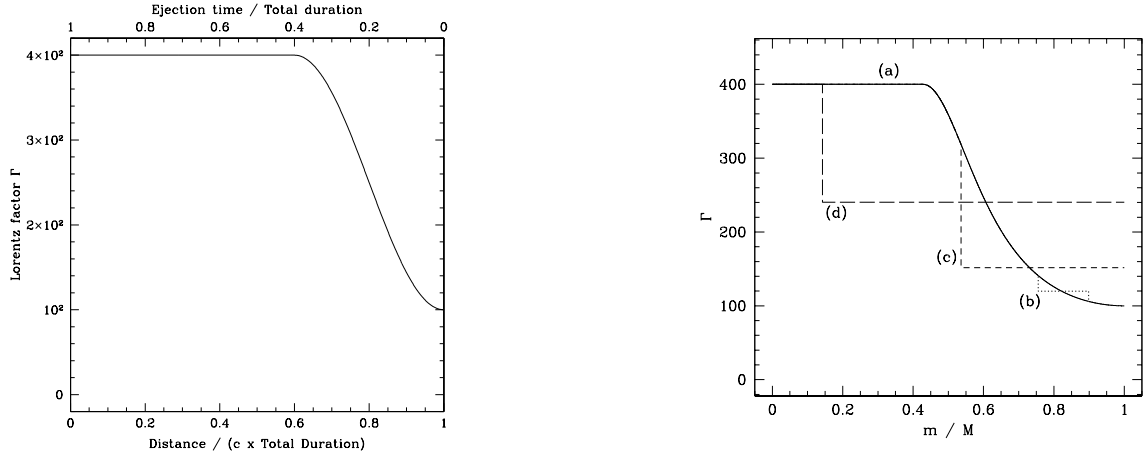

Fig. 1. Dynamics of internal shocks : an example. Left: initial distribution of Lorentz factors within the relativistic outflow, which is discretized in several hundreds of shells. Right: the distribution of the Lorentz factor at different times in Lagrangian coordinates m/M (M being the total mass of the wind): (a) the distribution just before the shock formation; (b) two shocks are formed, one arriving on the front of the wind at time t_F, and the other arriving on the back at t_B; (c) $t>t_F$, the front shock has reached the front of the wind and the reverse shock continues its propagation; (d)$t<t_R$, just before the reverse shock has reached the rear end of the wind.

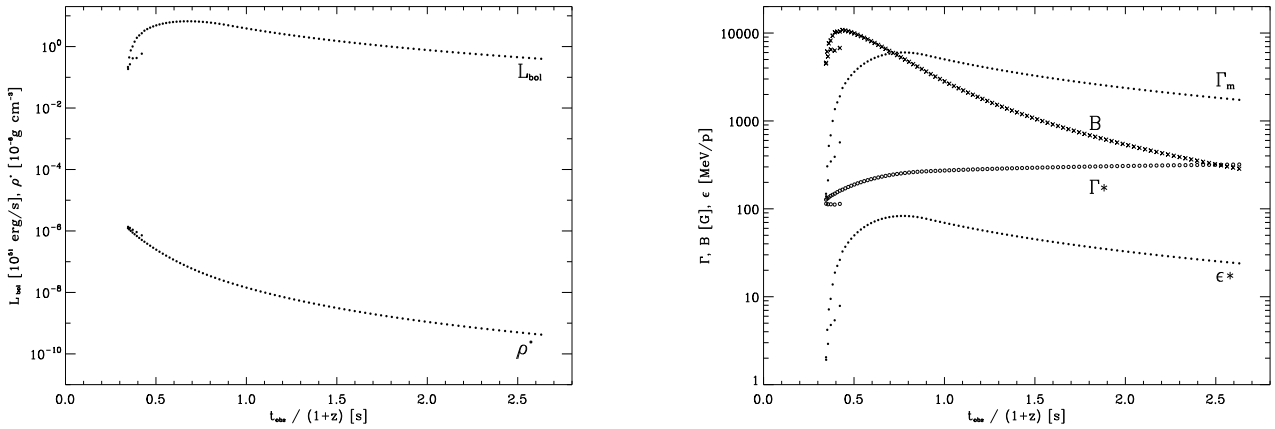

Fig. 2. Physical conditions in the shocked medium. The isotropic luminosity L_{bol} and the comoving density ρ_* (left panel), the Lorentz factor Γ_*, the comoving specific energy density ϵ_*, the minimum Lorentz factor Γ_m of the accelerated electrons and the amplified magnetic field B (right panel) are plotted as a function of the arrival time of photons in the observer frame, for the same case as in Fig. 1. The parameters selected for this simulation were α_e=1/3, ξ=0.003, α_B=1/3 and the total (isotropic equivalent) injected kinetic energy E=10^{54} erg. Such a small fraction of accelerated electrons is considered in order to have large enough Γ_m and the gamma–rays in the emergent spectrum produced by synchrotron emission.

2.2 Radiative processes in the shocked medium

We have developed a code to compute the emission in the comoving frame of the shocked material. The calculation is done for all the collisions occurring during the dynamical evolution of the relativistic flow. For one shocked shell, the radiative processes (including the cooling of the shocked material by the spherical adiabatic expansion) shell) are followed starting immediately after the collision. The requirement of the model is that relativistic electrons lose their energy via radiation on a radiative timescale t'_{rad} that is much smaller from the radiative timescale t'_{ex}=R/Γ_*c in order to have high radiative efficiency. It also implies that electron and photon

distribution are evolving strongly in time; we follow the time evolution of the electron density $n'_e(\Gamma'_e, t')$ and the photon density $n'_{\nu'}(t')$ accounting for the following processes: adiabatic cooling, synchrotron radiation, inverse Compton scattering, synchrotron self-absorption and $\gamma\gamma$ annihilation:

$$\frac{\partial n'}{\partial t'}(\Gamma'_e, t') = -\frac{\partial}{\partial \Gamma'_e}\Big[\Big(\frac{d\Gamma'_e}{dt'}\Big|_{syn+ic} + \frac{d\Gamma'_e}{dt'}\Big|_{ad}\Big) n'(\Gamma'_e, t')\Big] \tag{2.1}$$

$$\begin{aligned}\frac{\partial n'_\nu}{\partial t'} &= \int n'(\Gamma'_e, t') P_{syn+ic}(\Gamma'_e) d\Gamma'_e - c n'_\nu \int n'(\Gamma'_e, t') \sigma_{abs}(\Gamma'_e, \nu) d\Gamma'_e - \\ &\quad - c n'_\nu \int_{\nu' > \frac{(m_e c^2)^2}{h^2 \nu}} n'_{\nu'}(t') \sigma_{\gamma\gamma}(\nu, \nu') d\nu' \end{aligned} \tag{2.2}$$

This evolution is computed for a duration of the order of the dynamical timescale t'_{ex} (Fig. 3). The photon spectrum n'_ν at t'_{ex} is the final contribution of the shocked shell to the observed radiation. We explain in the next subsection how all these elementary contributions are added to produce a complete GRB.

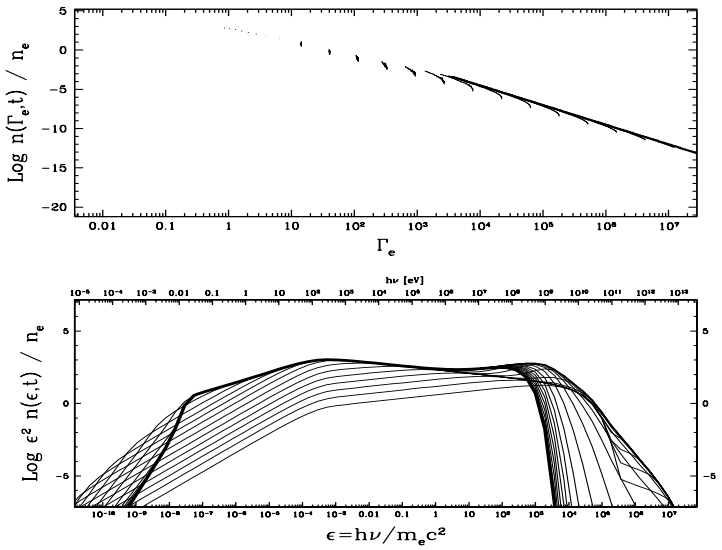

Fig. 3. Emission in the comoving frame of the shocked medium. The time evolution of the electron distribution (upper panel) and photon spectrum (lower panel) is plotted during a dynamical timescale t'_{ex}. The initial electron distribution is plotted with the thick solid line; on the lower panel, the thick line presents the final photon spectrum emerging from the shell. This simulation was done using the parameters: R=1.5×10^{15}, Γ_*=290, Γ_m=3555, B=512 G and n_e=1.3×10^8. These parameters are not typical for GRBs but allow a clear identification of all processes : the first peak is due to the synchrotron radiation (with a signature of the self-absorption at low frequency) and the second peak is due to inverse Compton scattering, with -in addition- a cutoff at high energy due to $\gamma\gamma$ annihilation.

2.3 Observed time profiles and spectrum

The overall burst spectrum and time profiles are obtained by adding up the contributions arising from all the internal elementary shocks that occur during the expansion of the wind. Each spectrum in the time evolution (that was calculated in the comoving frame of the shocked shell, see Fig. 3) was transformed to the observer frame accounting for the relativistic effects, the geometry (i.e. the curvature of the emitting surface) and cosmological effects (assuming that the burst was located at redshift z=1).

In the following example we have adopted the initial profile for the Lorentz factor in the wind as presented in Fig. 1. The injected energy was $\dot{E}=10^{54}$erg/s, that for an efficiency of conversion into gamma–rays of $\sim$6.5%

and a burst lasting ∼4 seconds, yields a total energy ≈10^{52}erg. The parameters selected for this simulation were α_e=1/3, ξ=0.003, α_B=1/3 (see Fig. 2). The instantaneous spectra obtained for arrival times (time at the observer) 1.0, 1.5 and 3.5 seconds are shown in Fig. 4. In this simple example the spectral evolution is clearly evident in terms of the peak energy of the spectrum and the high energy spectral cut-off.

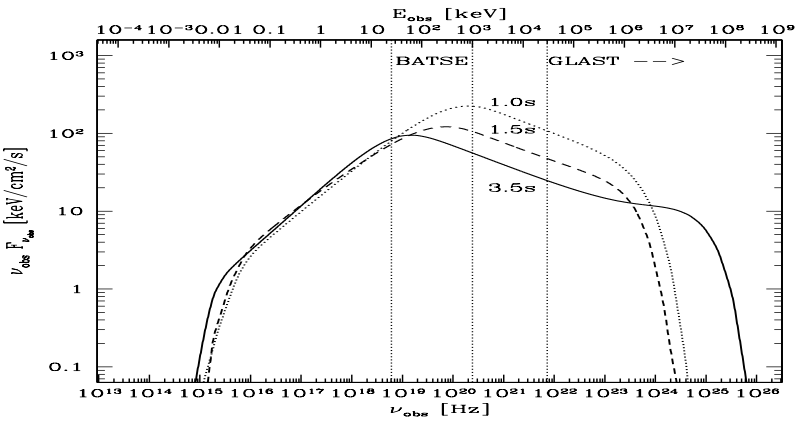

Fig. 4. Observed spectra corresponding to arrival times 1.0 (dotted line), 1.5 (dashed line) and 3.5 seconds (solid line). In this plot all the spectral components are taken into account (i.e. synchrotron emission, inverse Compton scattering, self-absorption and $\gamma\gamma$ annihilation component).

The light curves at low- and high- gamma–ray energy range as well as the global spectrum are shown in Fig. 5. The high energy component is dominated by the tail of the synchrotron emission and an additional inverse Compton component. However it appears at late arrival times because of a strongly evolving high energy cut-off due to $\gamma\gamma$ annihilation. This evolution is caused by several factors: the evolution of the bulk Lorentz factor, the optical depth and the evolution of the peak energy of the spectrum of synchrotron photons. Such effects are crucial for the observations of the high-energy (>0.1 GeV) part of the spectrum and can be used for the diagnostic of the radiation mechanism at work.

3 Conclusion

We have developed the modelling tools that allow us to compute the gamma–ray burst emission in a time-dependant way in the different spectral bands, under the assumption that GRBs originate from the dissipation of energy in the internal shocks formed within the relativistic wind. The emphasis of this work is given to the processes that favour the high–energy emission; the understanding of high–energy spectral behaviour allows also the identification of the processes responsible for the emission in lower energy bands. Further exploration of the parameter (such as α_e, α_B, ξ) space of the internal shock model will be used to make predictions on the GLAST observations and to asses the physical diagnostics for the measurement of parameters such as the bulk Lorentz factor, the magnetic field or the mean electron Lorentz factor.

References

Asano, K. & Inoue, S. 2007, astro-ph/0705.2910v2
Atkins, R. et al. 2000, ApJ, 533, L119
Baring, M.G. 2006, ApJ, 650, 1004
Bykov, A. & Mészáros, P. 1996, ApJ, 461, L37
Daigne, F. & Mochkovitch, R. 1998, MNRAS, 296, 275
Gupta, N. & Zhang, B. 2007, astro-ph/0704.1329v1
Hurley, K., et al. 1994, Nature, 372, 652
Paciesas, W.S. et al. 1999, ApJSS, 122, 465
Rees, M.J. & Mészáros, P. 1994, ApJ, 430, L93.

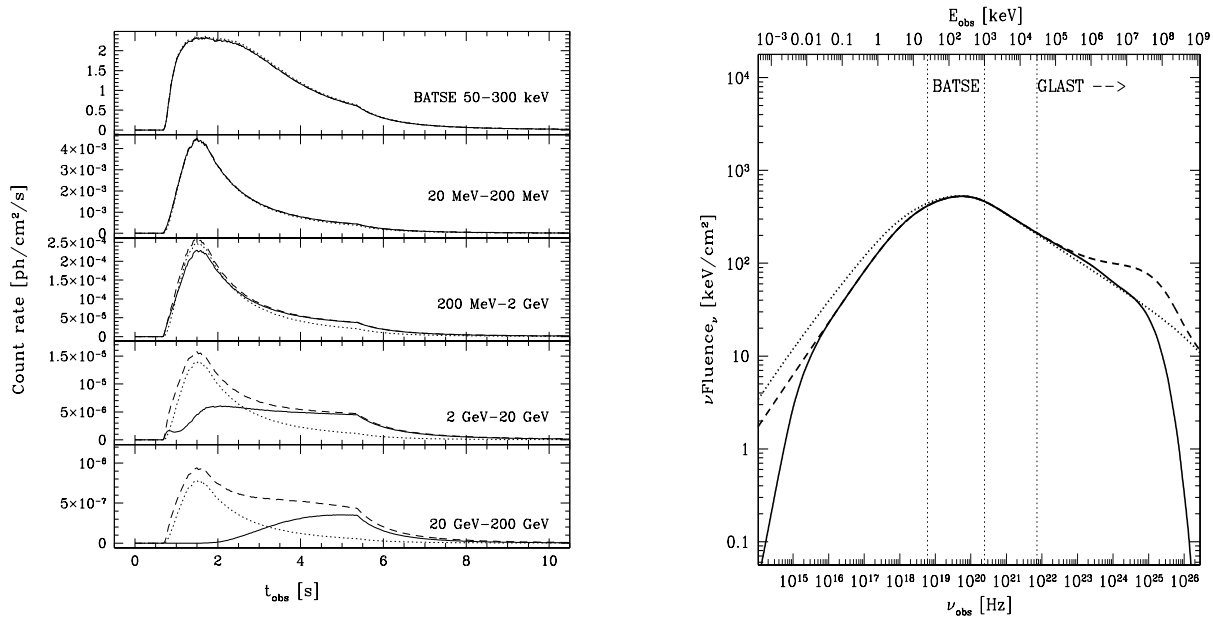

Fig. 5. Light curves for different energy bands (right panel) and the time-integrated spectrum (left panel) for the example described in the text; the contributions of different emission mechanisms are distinguished. Dotted line presents the contribution of synchrotron photons only; the dashed line shows how the inverse Compton scattering influences the spectrum. The final spectrum, with $\gamma\gamma$ annihilation apparent at high energies and self-absorption at low energies, is shown by the solid line. The same notation applies to both panels.